

# Atomically thin obstructed atomic insulators with robust edge modes and quantized spin Hall effect

Rahul Verma and Bahadur Singh\*

*Department of Condensed Matter Physics and Materials Science,  
Tata Institute of Fundamental Research, Colaba, Mumbai 400005, India*

Symmetry-protected edge states serve as direct evidence of nontrivial electronic topology in atomically thin materials. Finding these states in experimentally realizable single-phase materials presents a substantial challenge for their use for both fundamental studies and developing functional nanoscale devices. Here, we show the presence of robust edge states in phosphorene and group-Va monolayers with puckered lattice structures. By carefully analyzing the symmetry of the atomic sites and edge modes properties, we demonstrate that these atomically thin two-dimensional (2D) materials realize recently introduced obstructed atomic insulator states with partially occupied edge modes. The obstructed edge modes attain a Rashba-type spin splitting with Rashba parameter ( $\alpha$ ) of 1.52 eV Å for arsenene. Under strain or doping effects, these obstructed insulators transition to a phase with substantial spin-Berry curvature, yielding a double quantum spin Hall state with a spin Hall conductivity of  $4\frac{e^2}{h}$ . The experimental availability of phosphorene and other group-Va materials featuring puckered lattice structures could enable verification of obstructed atomic states and enhanced spin-Berry curvature effects discussed in this study, offering the potential for applications in topological electronic and spintronic devices.

*Introduction.* Coupling of electron topology, spin, and orbital degrees of freedom is the foundation of topological quantum materials having desirable disorder-resistant states [1–3]. The nontrivial topological state is generally driven by a bulk band inversion at high symmetry points in the Brillouin zone (BZ) and thus, the information of electronic wavefunction symmetries at these high-symmetry points is enough to diagnose the topology of a material as proposed in theory of topological quantum chemistry or symmetry indicators [4–7]. Especially, within topological quantum chemistry, the band representations (BRs) of occupied states of a material can be expressed as a linear combination of the elementary band representations (eBRs, also known as the basis of atomic limit) at high-symmetry points. When specific coefficients of this linear combination of eBRs are rational fractions, the material is a topological insulator or topological semimetal. Conversely, if these coefficients are non-negative integers, the material is a trivial insulator [7–10]. The topologically trivial insulators can also support unconventional surface states if their electrons occupy atom-unoccupied Wyckoff positions such that the BRs cannot be induced only from atom-centered band representations (aBRs) [11–13]. Such insulators, dubbed as obstructed atomic insulators (OAIs), host electronic states with filling anomaly at surfaces cleaved at atom-unoccupied Wyckoff positions [13]. The OAIs have been predicted in three-dimensional (3D) materials and verified recently in SrIn<sub>2</sub>P<sub>2</sub> and elemental silicon [14, 15]. The OAIs hold great promise for realizing exotic states such as higher-order topological states, unconventional superconductivity, and electrides with superior catalytic properties useful for quantum science and technological applications [16–24].

The atomically thin 2D materials provide an unprece-

dent framework for investigating topological quantum phenomena under carrier confinement that can be further manipulated by external strain, electric field, and/or doping effects [25–28]. Among various families of 2D materials, phosphorene and group-Va materials with puckered honeycomb lattice are mechanically exfoliated to the monolayer limit [27–33]. They show a thickness-dependent bandgap which is further sensitive to external electric field and surface doping effects. Specifically, a topologically nontrivial Dirac semimetal state is realized in phosphorene via potassium surface doping or under a vertical electric field [34–37]. The other group-Va monolayer layers as one moves down the periodic table (P→As→Sb) show a topological phase transition to a state with multiple unpinned Dirac cones and puzzling intertwining edge states [33, 38, 39]. Despite these studies, it is unclear if these 2D materials can support OAIs with conducting edge modes, and how the edge modes evolve across the periodic table in these materials.

In this paper, we report the theoretical prediction of the OAI state with spin-filtered edge modes in monolayers of group-Va materials with puckered honeycomb lattice. Through a systematic analysis of the bulk and edge energy spectra combined with symmetry analysis, we illustrate that phosphorene and group-Va monolayers exhibit half-filled obstructed states along both armchair and zigzag edges. The obstructed edge states (OESs) exhibit a finite Rashba-type spin-splitting with a Rashba coupling constant of  $\alpha = 1.52$  eV Å for Arsenene. We discuss the evolution of OESs from P to As and Sb and show that due to a generic point band inversion in Sb, these states evolve to form gapless double quantum spin Hall states in Sb with quantized spin Hall conductivity of  $\sigma_{xy}^z = 4\frac{e^2}{h}$ . Such topological phase transition can be captured by applying uniaxial strain in Arsenene. We

further demonstrate that these materials respect spin  $U(1)$  quasi-symmetry which ascertains a quantized spin Hall conductivity and two pairs of spin-polarized counter-propagating topological edge states.

*Crystal structure and OAI identification.* We start discussing the puckered honeycomb structure of phosphorene, which is a single layer of bulk black phosphorus. Phosphorene consists of two stacked P zigzag chains such that each P atom forms three bonds with its nearest neighbor atoms (Fig. 1(a)). Such a bonding configuration drives a non-symmorphic  $Pmna$  space group (#53). It respects inversion  $\mathcal{I} : (x, y, z) \rightarrow (-x, -y, -z)$ , a vertical mirror plane  $\mathcal{M}_y : (x, y, z) \rightarrow (x, -y, z)$  perpendicular to the zigzag direction and two-fold rotations  $\tilde{\mathcal{C}}_{2x} : (x, y, z) \rightarrow (x + \frac{1}{2}, -y + \frac{1}{2}, -z)$ ,  $\mathcal{C}_{2y} : (x, y, z) \rightarrow (-x, y, -z)$ ,  $\tilde{\mathcal{C}}_{2z} : (x, y, z) \rightarrow (-x + \frac{1}{2}, -y + \frac{1}{2}, z)$  and glide mirror  $\tilde{\mathcal{M}}_x : (x, y, z) \rightarrow (-x + \frac{1}{2}, y + \frac{1}{2}, z)$  and  $\tilde{\mathcal{M}}_z : (x, y, z) \rightarrow (x + \frac{1}{2}, y + \frac{1}{2}, -z)$  symmetries. P atoms occupy  $4h : \{(0, y, z), (0, -y, -z), (\frac{1}{2}, -y, z + \frac{1}{2}), (\frac{1}{2}, y, -z + \frac{1}{2})\}$  Wyckoff position in the lattice that induces 4 (8) BRs of single (double) space group. There are two additional Wyckoff positions  $2c : \{(\frac{1}{2}, \frac{1}{2}, 0), (0, \frac{1}{2}, \frac{1}{2})\}$  and  $4g : \{(\frac{1}{4}, y, \frac{1}{4}), (\frac{1}{4}, -y, \frac{3}{4}), (\frac{3}{4}, -y, \frac{3}{4}), (\frac{3}{4}, y, \frac{1}{4})\}$  in lattice that are not occupied by atoms. Considering 5 valence electrons of P and any group-Va element, the phosphorene lattice has 20 valence electrons. This satisfies a condition for filling-enforced OAI,  $N_e = 8N + 4$ , where  $N \in \mathbb{Z}$ , for space group  $Pmna$  [11]. This implies that the decomposition of BR into eBRs should include BRs generated from atom-unoccupied Wyckoff positions.

To identify the BRs of unoccupied Wyckoff positions, we present the band structure of phosphorene in Fig. 1(b) (see SMs for calculational details). The valence and conduction bands are well separated with an energy gap, dictating an insulator ground state. A mapping of irreducible representations (IRs) of occupied bands by considering the eBRs of single-space group reveals that  $s$  bands belong to BRs induced from atom-occupied Wyckoff position  $4h$  (marked as  $A'@4h$  in Fig. 1(b)). The remaining  $p$ -type bands belong to BRs that are generated from atom-unoccupied Wyckoff positions  $2c$  and  $4g$  ( $A_g@2c$  and  $A@4g$ ). This is more resolved in real-space charge localization of band representations in Fig. 1(c). Specifically, the electronic charge density arising from BRs of  $A_g@2c$  and  $A@4g$  at  $X$  point are localized on the empty Wyckoff positions  $2c$  and  $4g$ , respectively. In contrast, the charge density of  $A'@4h$  states is centered at atom-occupied Wyckoff position  $4h$ . The bands with  $p$  orbital character in phosphorene thus arise from unoccupied or obstructed atomic sites in the lattice.

We further evaluate the single-valued real space invariant (RSI)  $\delta_1$  at Wyckoff positions  $2c$ ,  $4g$ , and  $4h$  of space group  $Pmna$  to elucidate the OAI state [13]. The RSI index at each Wyckoff position is defined as  $\delta_1@2c = -m(A_g) + m(A_u) - m(B_g) + m(B_u)$ ,  $\delta_1@4g =$

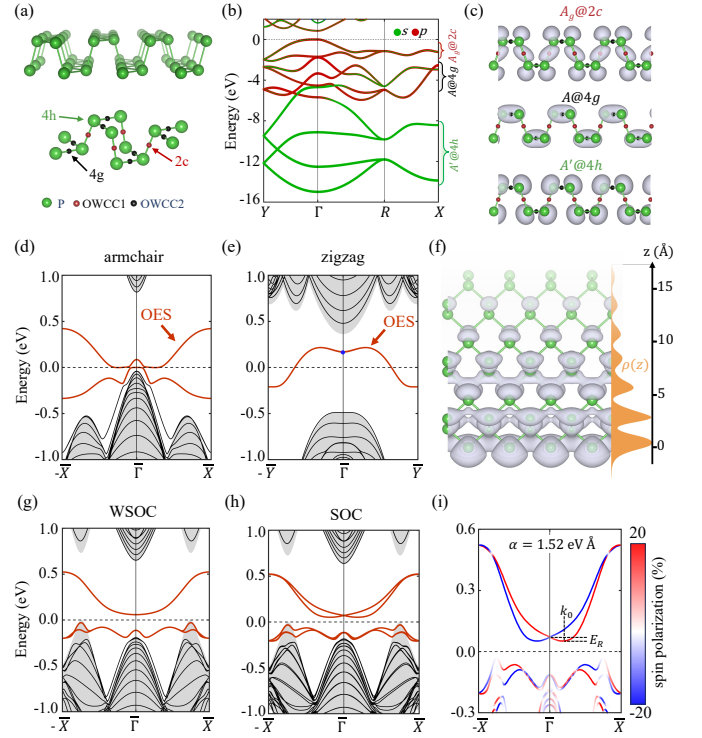


FIG. 1. (a) Puckered honeycomb lattice of phosphorene with Wyckoff positions  $4h$  (green),  $2c$  (red), and  $4g$  (black).  $4h$  Wyckoff position is atom occupied, whereas  $2c$  and  $4g$  positions are unoccupied (OWCC). (b) Orbital resolved band structure of phosphorene without spin-orbit coupling (SOC). Green and red colors identify P  $s$  and  $p$  states, respectively. BRs of occupied bands is shown. (c) Electronic charge density at  $X$  point arising from the BRs of  $A_g@2c$ ,  $A@4g$ , and  $A'@4h$  (see text for details). The maximum charge for  $A_g@2c$  and  $A@4g$  BRs is centered at atom unoccupied positions  $2c$  and  $4g$ . (d)-(e) Edge spectrum of phosphorene for (d) armchair and (e) zigzag edges. The shaded gray region identifies projected bulk bands, and red lines mark the OESs. (f) Electronic charge density ( $\rho$ ) of OESs at the  $\bar{\Gamma}$  point for zigzag edge (blue circle in (e)). The right panel shows the variation of  $\rho$  as a function of slab thickness  $z$  in orange. The vertical distance is calculated from the bottom phosphorus atom. Band structure of Arsenene (g) without and (h) with SOC along the armchair edge. (i) Spin texture of OESs along the armchair edge for Arsenene. Blue and red colors indicate up and down spin channels of  $S_z$ .  $k_0$  and  $E_R$  denote momentum and energy offsets of spin-split states.

$-m(A) + m(B)$ , and  $\delta_1@4h = -m(A') + m(A'')$ , where  $m(\rho)$  is the number of eBRs ( $\rho$ ) induced from a Wyckoff position. We obtain  $\delta_1@2c = -1$ ,  $\delta_1@4g = -1$ , and  $\delta_1@4h = -2$ . The non-zero integer values of RSI at  $2c$  and  $4g$  confirm the OAI phase in phosphorene. A similar analysis holds for all other group-Va monolayers with a puckered lattice. The nontrivial RSI index indicates that these monolayers will support robust states over edges that cut through unoccupied Wyckoff positions.

In Figs. 1(d) and 1(e), we present the first-principles

edge band structure of phosphorene terminated at  $2c$  (zigzag edge) and  $4g$  (armchair edge) sites without SOC. Both edges support the partially filled conducting states within the 2D bulk energy gap. Notably, the OESs do not connect the bulk valence and conduction bands and thus, are distinct from quantum spin Hall insulators where the helical edge states connect the bulk valence and conduction bands. Regardless, the OESs cross the Fermi level, exhibiting the filling anomaly [11–13]. Figure 1(f) illustrates the distribution of the electronic charge density associated with OESs at  $\bar{\Gamma}$  point for the zigzag edge and its variation as a function of slab thickness ( $z$ ). The electronic charge density is localized at the slab edge and decays exponentially into the bulk as expected for edge states. We further show the OESs of arsenene in Figs. 1(g)-1(i). Due to a slightly larger SOC, the OESs in Arsenene are spin-polarized with SOC. They show a Rashba-type spin splitting with maximum energy offset of  $E_R = 0.019$  eV at  $k_0 = 0.025$   $\text{\AA}^{-1}$  with a Rashba constant  $\alpha = \frac{2E_R}{k_0} = 1.52$  eV $\text{\AA}$ .

*Hidden structural and topological phase transition.* We now discuss the evolution of electronic structure from monolayer P to Sb and reveal a unique topological phase transition. In Figs. 2(a)-2(c), we present the orbital-resolved band structures of these monolayers in the vicinity of the Fermi level. Although the band structure stays insulating from P to Sb along the high-symmetry directions, there are subtle changes in it. The valence and conduction band extremum is shifted from the  $\Gamma$  point in P to a generic momentum point in Sb. The bands consist of  $p_z$  orbital at the  $\Gamma$  point whereas they are comprised of  $p_x$  orbitals along  $\Gamma - X$  direction. These  $p_x$  bands change dispersion from parabolic in P and As to almost linear and gapless in Sb. Figure 2(d) illustrates the energy dispersion of Sb in the full 2D BZ. Interestingly, the  $p_x$  bands remain gapless across the  $\Gamma - X$  line, forming four Dirac cones on the  $k_x - k_y$  plane. These Dirac cones are located at generic momenta ( $\pm 0.38 \frac{2\pi}{a}, \pm 0.02 \frac{2\pi}{b}$ ) as resolved in the constant energy contours in Fig. 2(e). The SOC effects open a hybridization gap at the Dirac nodes, leading to an inverted band structure with band inversion at generic  $k$  points (Fig. 2(f)).

In Fig. 2(g), we present the wannier charge centers (WCCs) spectrum of the occupied states of P and Sb. The WCCs spectrum shows adiabatically distinct characteristics, remaining gapful for P and gapless for Sb. Despite these features, the WCCs spectrum reveals  $\mathbb{Z}_2$  trivial connectivity for both P and Sb, thereby dictating a  $\mathbb{Z}_2 = 0$  trivial state. The topological  $\mathbb{Z}_2$  trivial state is further verified through the parity analysis of occupied bands at high-symmetry points. The presence of a band inversion and the WCCs connectivity in Sb signals a nontrivial electronic state distinct from P. However, since the band inversion happens at generic  $k$  points, it does not alter IRs of occupied bands at the high-symmetry points. Such a topological state is hidden

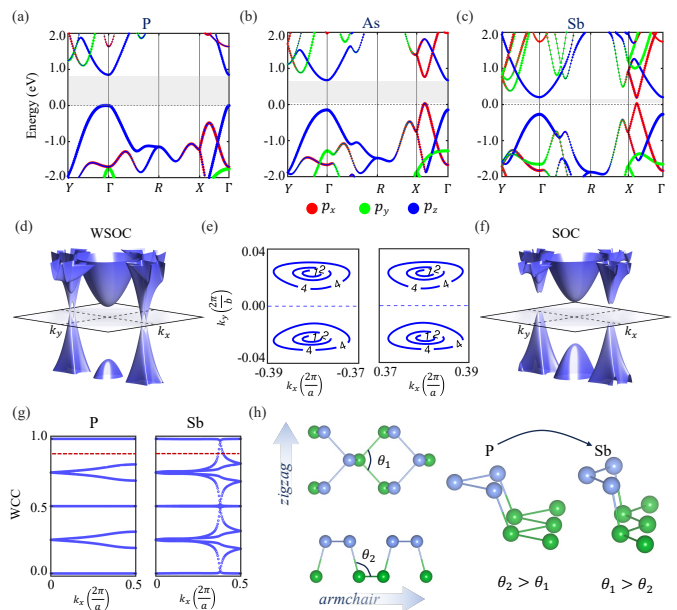


FIG. 2. Band structure of monolayer (a) P, (b) As, and (c) Sb with puckered honeycomb lattice without SOC. Red, green, and blue identify  $p_x$ ,  $p_y$ , and  $p_z$  orbitals. Bulk energy gap is marked in shaded gray. (d)  $E - k_x - k_y$  energy dispersion and (e) constant energy contours of Sb without SOC. Four Dirac points at generic  $k$  points are resolved. Numbers on curves in (e) mark the contour energy in meV. (f)  $E - k_x - k_y$  energy dispersion of Sb with SOC showing a hybridization gap at Dirac points. (g) WCC spectrum for P and Sb. WCCs cross the arbitrary red dashed line an even number of times for Sb. (h) Evolution of crystal lattice from P to Sb with increased puckering. Green and blue spheres identify atoms on two different planes.  $\theta_1$  and  $\theta_2$  define in-plane and out-of-plane angles (left). Two geometric configurations exposing hidden structural transition from P to Sb (right).

from symmetry-indicator and TQC theories, and therefore, P, As, and Sb share the same topological characterization [38, 39].

We emphasize that the emergence of electronic structure from P to Sb has a strong correlation with their puckered lattice geometry and signals a hidden structural transition. To facilitate this analysis, we define bond angles  $\theta_1$  and  $\theta_2$  in the puckered lattice as shown in Fig. 2(h).  $\theta_1$  is an in-plane angle in the zigzag layer and  $\theta_2$  is the out-of-plane angle along the armchair direction, describing the non-planar puckering of the lattice.  $\theta_1$  and  $\theta_2$  are  $95.97^\circ$  and  $103.87^\circ$  for P and  $96.04^\circ$  and  $95.67^\circ$  for Sb, respectively. This indicates that the in-plane bond angle  $\theta_1$  is smaller than the non-planar bond angle  $\theta_2$  ( $\theta_1 < \theta_2$ ) for P with less puckering. This bond angle order is reversed for Sb with  $\theta_1 > \theta_2$  with large puckering. The electronic phase transition happens when  $\theta_1 \sim \theta_2$ . Importantly, when  $\theta_1 \sim \theta_2$ , each atom shares an isotropic electronic environment similar to graphene, thereby forming two critical points on the

$\Gamma - X$  line without SOC. When  $\theta_1 > \theta_2$ , each critical point splits into two Dirac points across the  $\Gamma - X$  line as seen in Sb.

A similar topological phase transition can also happen in As under the application of uniaxial strain along the zigzag direction. In Figs. 3(a)-3(c), we present the calculated band structure of As at various values of strain. We change the lattice parameter  $b$  along the zigzag direction (see SM for details). When  $b' = 1.10b$ , the valence and conduction bands have a parabolic energy dispersion with minimum along  $\Gamma - X$  direction. With an increase in  $b'$ , the valence and conduction bands start approaching each other and cross at  $\Gamma - X$  line for  $b' = 1.12b$  (Fig. 3(b)). With a further increase in  $b'$ , four Dirac cones appear at the generic  $k$  points across the  $\Gamma - X$  line. In Figs. 3(d)-3(e), we present WCCs spectrum of As for  $b' = 1.10b$  and  $b' = 1.14b$  with SOC. The WCCs spectrum resolves distinct characteristics with a  $\mathbb{Z}_2 = 0$  trivial phase. However, a strong spin-Berry curvature is found near the gapped Dirac nodes for As with generic  $k$  point band inversion (Fig. 3(f)).

To explore the emergence of OESs with strain, we present the calculated armchair edge spectrum in Figs. 3(g)-3(i) for  $b' = 1.10b$ ,  $b' = 1.12b$ , and  $b' = 1.14b$ . The two pairs of OESs are seen within the bulk gap in the vicinity of the Fermi level for  $b' = 1.10b$  (Fig. 3(g)). These OESs evolve to form gapless Dirac-type states within the bulk band inversion at generic  $k$  points, forming double quantum spin-Hall edge states.

*Helical spin-texture and quantized spin Hall effect.* The preceding discussion made it clear that although Sb or strained As are OAI based on the analysis of IRs at high-symmetry points, they host a topologically distinct band structure than P or As. Their OESs form a gapless Dirac-type energy dispersion within the bulk gap. In Figs. 4(a)-4(b), we show the spin texture of these edge states for Sb and As with  $b' = 1.14b$ . The two pairs of oppositely spin-polarized edge states are evident along  $-\bar{X} - \bar{\Gamma} - \bar{X}$  direction. They have a dominant  $S_z$  spin component and thus, preserve a spin U(1) quasi-symmetry (see SMs). Notably, owing to the presence of time-reversal symmetry and  $C_{2y}$  symmetry along the armchair edge, the edge states can support both  $S_x$  and  $S_z$  spin components. However, we find that  $S_x$  here is negligible. Such spin-symmetry leads to gapless edge states and can support perfectly quantized spin Hall conductivity. In Fig. 4(c), we show a schematic representation of the gapless Dirac-type edge states as seen in Sb or strained As with  $b' > 1.12b$ .

Figure 4(d) illustrates the calculated intrinsic spin Hall conductivity (SHC)  $\sigma_{xy}^z$  as a function of the Fermi energy for As and Sb. The SHC is calculated using the Kubo formula  $\sigma_{xy}^z = \frac{-e^2}{\hbar} \frac{1}{A} \sum_{\mathbf{k}} \Omega_{xy}^z(\mathbf{k})$  [40, 41]. Here,  $\Omega_{xy}^z(\mathbf{k}) = \sum_n f_n(\mathbf{k}) \Omega_{n,xy}^z(\mathbf{k})$  is the  $k$ -resolved spin Berry curvature and  $\Omega_{n,xy}^z(\mathbf{k}) = \hbar^2 \sum_{m \neq n} \frac{-2\text{Im}\langle n\mathbf{k} | \hat{J}_x^z | m\mathbf{k} \rangle \langle m\mathbf{k} | \hat{v}_y | n\mathbf{k} \rangle}{(E_{n\mathbf{k}} - E_{m\mathbf{k}})^2}$  gives the band resolved spin Berry curvature in 2D BZ with

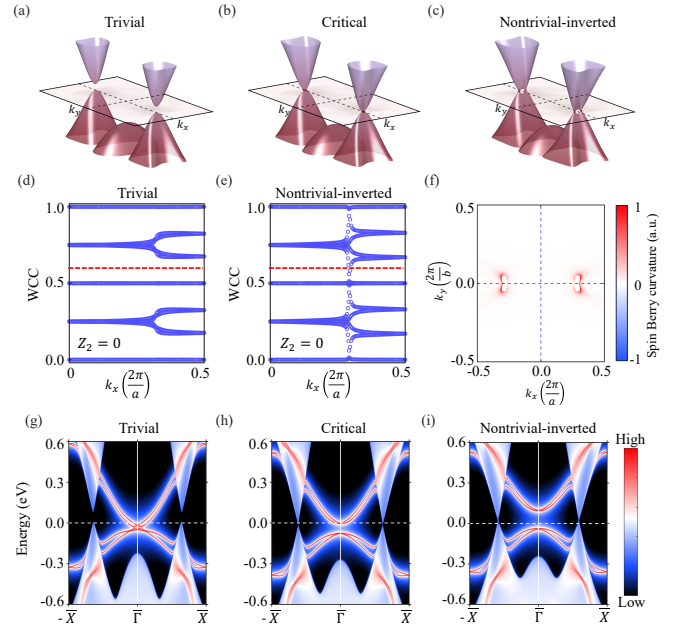


FIG. 3. Calculated  $E - k_x - k_y$  band structure of strained As without SOC for (a)  $b' = 1.10b$ , trivial phase, (b)  $b' = 1.12b$ , critical phase, and (c)  $b' = 1.14b$ , nontrivial-inverted phase.  $b$  is the lattice parameter along the zigzag direction. Dashed lines on the plane mark  $k_x$  and  $k_y$  principal axes of 2D BZ. Evolution of WCCs for (d)  $b' = 1.10b$ ; trivial phase and (e)  $b' = 1.14b$ ; nontrivial-inverted phase. (f) Spin-Berry curvature obtained for  $b' = 1.14b$ , showing hotspots at the hybridized Dirac nodes. Calculated semi-infinite edge spectrum of As for (g)  $b' = 1.10b$ , (h)  $b' = 1.12b$ , and (i)  $b' = 1.14b$ . OESs evolve from gapped to gapless on the  $\bar{\Gamma} - \bar{X}$  line.

area  $A$ .  $E_{n\mathbf{k}}$  represents the energy of Bloch state  $|n\mathbf{k}\rangle$  with occupation  $f_n(\mathbf{k})$ . The spin current operator is defined as  $\hat{J}_x^z = \frac{1}{2} \{ \hat{\sigma}_z, \hat{v}_x \}$ , where  $\hat{\sigma}_z$  is the spin operator and  $\hat{v}_x$  is the velocity operator.  $\sigma_{xy}^z$  represents  $z$ -polarized spin-current along  $x$  direction generated by an electric field along  $y$  direction. The SHC for the As is zero, whereas it has a quantized value of  $4\frac{e^2}{h}$  for Sb and strained As ( $b' > 1.12b$ ) in the bulk gap region. Such a large SHC arises due to strong spin-Berry curvature at the band inverted  $k$  points in both Sb and As<sub>NTI</sub> (Fig. 4(e)).

Generally, the SHC deviates from exact quantization due to nonconserved- $S_z$  Hamiltonians in materials [42–45]. However, as shown in Ref. [38], the group-Va monolayers host a unique SOC Hamiltonian  $H_{SOC} \propto q_y \sigma_z s_z$ , where  $q_y$  is momentum around Dirac node and  $\sigma_z$  and  $s_z$  are Pauli matrices acting on orbital and spin space. This  $H_{SOC}$  commutes with  $S_z$ , leading to a spin U(1) quasi-symmetry and perfect quantization of SHC as found here. Owing to the presence of  $S_z$  SOC Hamiltonian preserving spin U(1) quasi-symmetry, the associated topological state can be described by a spin-Chern number of 2 [43–46].

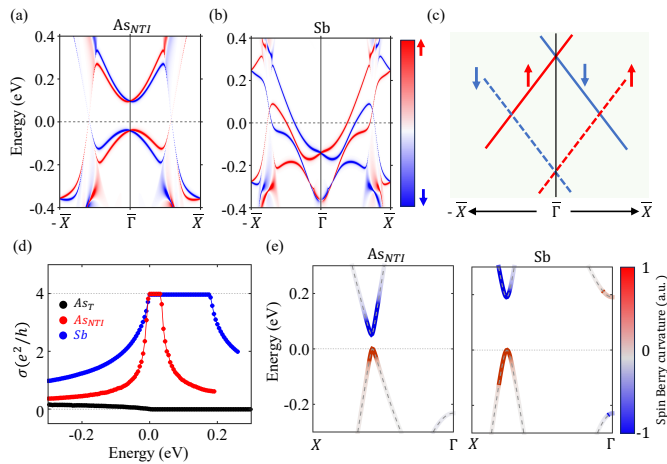


FIG. 4.  $S_z$  spin-component resolved edge spectrum of (a) nontrivially-inverted As ( $AS_{NTI}$ ) with  $b' = 1.14b$  and (b) Sb. Spin is nearly polarized along the  $z$  direction, maintaining spin  $U(1)$  quasi-symmetry. (c) Schematic representation of edge Dirac states along  $-\bar{X} - \Gamma - \bar{X}$  direction. Red and blue indicate spin-up and spin-down states polarized along the  $z$  direction. (d) Intrinsic SHC  $\sigma_{xy}^z$  for trivial and nontrivial phases of As and Sb. SHC is perfectly quantized to  $4\frac{e^2}{h}$  within the bulk energy gap. (e) Band resolved spin-Berry curvature along  $\Gamma - X$  direction for  $AS_{NTI}$  and Sb.

*Summary.* We demonstrate the presence of OAI state in phosphorene and related group-Va monolayers with a puckered lattice. The charge density of their occupied bands near the Fermi level is centered at atom-unoccupied Wyckoff positions. Such localization of charge centers leads to nontrivial RSI index and OESs on crystal edges that cut through the unoccupied Wyckoff positions. We show that OESs are spin-polarized for As having a Rashba-type spin splitting with Rashba parameter  $\alpha$  of  $1.52 \text{ eV \AA}$ . We resolve a unique topological state with generic  $k$  points band inversion in Sb and strained As and perfectly quantized SHC of  $4\frac{e^2}{h}$ . We argue that the perfect quantization of SHC arises because of a unique  $S_z$  conserved SOC Hamiltonian. Our work demonstrates that phosphorene and other group-Va monolayers would provide an ideal basis for exploring OAIs and enhanced spin-Berry curvature effects with potential applications in topological spintronics.

*Acknowledgements.* We thank Bikash Patra for the useful discussions. This work is supported by the Department of Atomic Energy of the Government of India under Project No. 12-R&D-TFR-5.10-0100 and benefited from the HPC resources of TIFR Mumbai.

\* Corresponding author: [bahadur.singh@tifr.res.in](mailto:bahadur.singh@tifr.res.in)

[1] M. Z. Hasan and C. L. Kane, Colloquium: Topological insulators, *Rev. Mod. Phys.* **82**, 3045 (2010).

- [2] Y. Tokura, M. Kawasaki, and N. Nagaosa, Emergent functions of quantum materials, *Nat. Phys.* **13**, 1056 (2017).
- [3] B. Singh, H. Lin, and A. Bansil, Topology and symmetry in quantum materials, *Adv. Mater.* **35**, 2201058 (2022).
- [4] J. Kruthoff, J. de Boer, J. van Wezel, C. L. Kane, and R.-J. Slager, Topological classification of crystalline insulators through band structure combinatorics, *Phys. Rev. X* **7**, 041069 (2017).
- [5] H. C. Po, A. Vishwanath, and H. Watanabe, Symmetry-based indicators of band topology in the 230 space groups, *Nat. Commun.* **8**, 50 (2017).
- [6] Z. Song, T. Zhang, Z. Fang, and C. Fang, Quantitative mappings between symmetry and topology in solids, *Nat. Commun.* **9**, 3530 (2018).
- [7] B. Bradlyn, L. Elcoro, J. Cano, M. G. Vergniory, Z. Wang, C. Felser, M. I. Aroyo, and B. A. Bernevig, Topological quantum chemistry, *Nature* **547**, 298 (2017).
- [8] L. Michel, Elementary energy bands in crystals are connected, *Phys. Rep.* **341**, 377 (2001).
- [9] J. Cano, B. Bradlyn, Z. Wang, L. Elcoro, M. G. Vergniory, C. Felser, M. I. Aroyo, and B. A. Bernevig, Building blocks of topological quantum chemistry: Elementary band representations, *Phys. Rev. B* **97**, 035139 (2018).
- [10] J. Cano, B. Bradlyn, Z. Wang, L. Elcoro, M. G. Vergniory, C. Felser, M. I. Aroyo, and B. A. Bernevig, Topology of disconnected elementary band representations, *Phys. Rev. Lett.* **120**, 266401 (2018).
- [11] Y. Xu, L. Elcoro, Z.-D. Song, M. G. Vergniory, C. Felser, S. S. P. Parkin, N. Regnault, J. L. Mañes, and B. A. Bernevig, Filling-enforced obstructed atomic insulators, *Phys. Rev. B* **109**, 165139 (2024).
- [12] J. Gao, Y. Qian, H. Jia, Z. Guo, Z. Fang, M. Liu, H. Weng, and Z. Wang, Unconventional materials: the mismatch between electronic charge centers and atomic positions, *Sci. Bull.* **67**, 598 (2022).
- [13] Y. Xu, L. Elcoro, G. Li, Z.-D. Song, N. Regnault, Q. Yang, Y. Sun, S. Parkin, C. Felser, and B. A. Bernevig, Three-dimensional real space invariants, obstructed atomic insulators and a new principle for active catalytic sites, (2021), [arXiv:2111.02433](https://arxiv.org/abs/2111.02433).
- [14] X.-R. Liu, H. Deng, Y. Liu, Z. Yin, C. Chen, Y.-P. Zhu, Y. Yang, Z. Jiang, Z. Liu, M. Ye, D. Shen, J.-X. Yin, K. Wang, Q. Liu, Y. Zhao, and C. Liu, Spectroscopic signature of obstructed surface states in  $\text{SrIn}_2\text{P}_2$ , *Nat. Commun.* **14**, 2905 (2023).
- [15] Y. Chen, Z. Liu, P. Deng, Y. Xu, H. Yang, D. Pei, C. Chen, S. He, D. Liu, S.-K. Mo, T. Kim, C. Cacho, H. Yao, Z. Song, X. Chen, Z. Wang, B. Yan, L. Yang, and B. Bernevig, Massive 1D Dirac line, solitons and reversible manipulation on the surface of a prototype obstructed atomic insulator, silicon [10.21203/rs.3.rs-2781859/v1](https://arxiv.org/abs/10.21203/rs.3.rs-2781859/v1) (2023).
- [16] D.-S. Ma, K. Yu, X.-P. Li, X. Zhou, and R. Wang, Obstructed atomic insulators with robust corner modes, *Phys. Rev. B* **108**, L100101 (2023).
- [17] W. A. Benalcazar, T. Li, and T. L. Hughes, Quantization of fractional corner charge in  $C_n$ -symmetric higher-order topological crystalline insulators, *Phys. Rev. B* **99**, 245151 (2019).
- [18] L. Wang, Y. Jiang, J. Liu, S. Zhang, J. Li, P. Liu, Y. Sun, H. Weng, and X.-Q. Chen, Two-dimensional obstructed atomic insulators with fractional corner charge in the

- $MA_2Z_4$  family, *Phys. Rev. B* **106**, 155144 (2022).
- [19] H. Sheng, Y. Xie, Q. Wu, H. Weng, X. Dai, B. A. Bernevig, Z. Fang, and Z. Wang, Majorana corner modes in unconventional monolayers of  $1T - PtSe_2$  family, (2023), [arXiv:2308.12055](https://arxiv.org/abs/2308.12055).
- [20] Z. Yang, H. Sheng, Z. Guo, R. Zhang, Q. Wu, H. Weng, Z. Fang, and Z. Wang, Superconductivity in unconventional metals, (2023), [arXiv:2306.08347](https://arxiv.org/abs/2306.08347).
- [21] P. Eck, C. Ortix, A. Consiglio, J. Erhardt, M. Bauernfeind, S. Moser, R. Claessen, D. Di Sante, and G. Sangiovanni, Real-space obstruction in quantum spin hall insulators, *Phys. Rev. B* **106**, 195143 (2022).
- [22] G. Li, Y. Xu, Z. Song, Q. Yang, Y. Zhang, J. Liu, U. Gupta, V. Sub, Y. Sun, P. Sessi, S. S. P. Parkin, B. A. Bernevig, and C. Felser, Obstructed surface states as the descriptor for predicting catalytic active sites in inorganic crystalline materials, *Adv. Mater.* **34**, 2201328.
- [23] S. Nie, Y. Qian, J. Gao, Z. Fang, H. Weng, and Z. Wang, Application of topological quantum chemistry in electrides, *Phys. Rev. B* **103**, 205133 (2021).
- [24] K. Jiang, Z. Qi, H. Weng, and J. Hu, Mottness in obstructed atomic insulators without mott transition, *Phys. Rev. B* **108**, 195102 (2023).
- [25] K. S. Novoselov, A. Mishchenko, A. Carvalho, and A. H. C. Neto, 2D materials and van der waals heterostructures, *Science* **353**, aac9439 (2016).
- [26] F. Sheng, C. Hua, M. Cheng, J. Hu, X. Sun, Q. Tao, H. Lu, Y. Lu, M. Zhong, K. Watanabe, T. Taniguchi, Q. Xia, Z.-A. Xu, and Y. Zheng, Rashba valleys and quantum hall states in few-layer black arsenic, *Nature* **593**, 56 (2021).
- [27] A. Carvalho, M. Wang, X. Zhu, A. S. Rodin, H. Su, and A. H. Castro Neto, Phosphorene: from theory to applications, *Nat Rev Mater* **1**, 1 (2016).
- [28] F. Xia, H. Wang, J. C. M. Hwang, A. H. C. Neto, and L. Yang, Black phosphorus and its isoelectronic materials, *Nat. Rev. Phys.* **1**, 306–317 (2019).
- [29] J. Kim, S. S. Baik, S. H. Ryu, Y. Sohn, S. Park, B.-G. Park, J. Denlinger, Y. Yi, H. J. Choi, and K. S. Kim, Observation of tunable band gap and anisotropic dirac semimetal state in black phosphorus, *Science* **349**, 723 (2015).
- [30] Q. Lu, K. Y. Chen, M. Snyder, J. Cook, D. T. Nguyen, P. V. S. Reddy, T.-R. Chang, S. A. Yang, and G. Bian, Observation of symmetry-protected dirac states in nonsymmorphic  $\alpha$ -antimonene, *Phys. Rev. B* **104**, L201105 (2021).
- [31] P. J. Kowalczyk, S. A. Brown, T. Maerkl, Q. Lu, C.-K. Chiu, Y. Liu, S. A. Yang, X. Wang, I. Zasada, F. Genuzio, T. O. Mentęs, A. Locatelli, T.-C. Chiang, and G. Bian, Realization of symmetry-enforced two-dimensional dirac fermions in nonsymmorphic  $\alpha$ -bismuthene, *ACS Nano* **14**, 1888 (2020).
- [32] R. Islam, B. Ghosh, C. Autieri, S. Chowdhury, A. Bansil, A. Agarwal, and B. Singh, Tunable spin polarization and electronic structure of bottom-up synthesized  $MoSi_2N_4$  materials, *Phys. Rev. B* **104**, L201112 (2021).
- [33] Q. Lu, J. Cook, X. Zhang, K. Y. Chen, M. Snyder, D. T. Nguyen, P. V. S. Reddy, B. Qin, S. Zhan, L.-D. Zhao, P. J. Kowalczyk, S. A. Brown, T.-C. Chiang, S. A. Yang, T.-R. Chang, and G. Bian, Realization of unpinned two-dimensional dirac states in antimony atomic layers, *Nat. Commun.* **13**, 4603 (2022).
- [34] B. Ghosh, B. Singh, R. Prasad, and A. Agarwal, Electric-field tunable dirac semimetal state in phosphorene thin films, *Phys. Rev. B* **94**, 205426 (2016).
- [35] S. S. Baik, K. S. Kim, Y. Yi, and H. J. Choi, Emergence of two-dimensional massless dirac fermions, chiral pseudospins, and berry's phase in potassium doped few-layer black phosphorus, *Nano Lett.* **15**, 7788 (2015).
- [36] Q. Liu, X. Zhang, L. B. Abdalla, A. Fazzio, and A. Zunger, Switching a normal insulator into a topological insulator via electric field with application to phosphorene, *Nano Lett.* **15**, 1222 (2015).
- [37] Z. J. Xiang, G. J. Ye, C. Shang, B. Lei, N. Z. Wang, K. S. Yang, D. Y. Liu, F. B. Meng, X. G. Luo, L. J. Zou, Z. Sun, Y. Zhang, and X. H. Chen, Pressure-induced electronic transition in black phosphorus, *Phys. Rev. Lett.* **115**, 186403 (2015).
- [38] Y. Lu, D. Zhou, G. Chang, S. Guan, W. Chen, Y. Jiang, J. Jiang, X. sen Wang, S. A. Yang, Y. P. Feng, Y. Kawazoe, and H. Lin, Multiple unpinned dirac points in group-Va single-layers with phosphorene structure, *Npj Comput. Mater.* **2**, 1 (2016).
- [39] B. Wang, X. Zhou, Y.-C. Hung, Y.-C. Lin, H. Lin, and A. Bansil, High spin-chern-number insulator in  $\alpha$ -antimonene with a hidden topological phase, *2D Mater.* **11**, 025033 (2024).
- [40] Y. Sun, Y. Zhang, C. Felser, and B. Yan, Strong intrinsic spin hall effect in the TaAs family of weyl semimetals, *Phys. Rev. Lett.* **117**, 146403 (2016).
- [41] J. Qiao, J. Zhou, Z. Yuan, and W. Zhao, Calculation of intrinsic spin hall conductivity by wannier interpolation, *Phys. Rev. B* **98**, 214402 (2018).
- [42] C. L. Kane and E. J. Mele,  $Z_2$  topological order and the quantum spin hall effect, *Phys. Rev. Lett.* **95**, 146802 (2005).
- [43] D. N. Sheng, Z. Y. Weng, L. Sheng, and F. D. M. Haldane, Quantum spin-hall effect and topologically invariant chern numbers, *Phys. Rev. Lett.* **97**, 036808 (2006).
- [44] E. Prodan, Robustness of the spin-chern number, *Phys. Rev. B* **80**, 125327 (2009).
- [45] L. Sheng, D. N. Sheng, C. S. Ting, and F. D. M. Haldane, Nondissipative spin hall effect via quantized edge transport, *Phys. Rev. Lett.* **95**, 136602 (2005).
- [46] L. Liu, Y. Liu, J. Li, H. Wu, and Q. Liu, Quantum spin hall effect protected by spin  $U(1)$  quasi-symmetry, (2024), [arXiv:2402.13974](https://arxiv.org/abs/2402.13974).